JOURNAL OF MATERIALS SCIENCE **40** (2005) 3891 – 3896

Electrical and structural characteristics of non-stoichiometric Cu-based delafossites

NATHAN A. ASHMORE, DAVID P. CANN*
Materials Science and Engineering Department, Iowa State University, Ames, Iowa 50011, USA
E-mail: batio3@iastate.edu

Non-stoichiometric Cu_xGaO_2 polycrystalline ceramics were prepared using solid-state synthesis methods and their structural and electrical properties were characterized as a function of *x*. While single phase delafossite could only be confirmed for the stoichiometric composition, X-ray diffraction results show that the *a* and *c* lattice parameters were stable from $Cu_{0.98}GaO_2$ to $Cu_{1.02}GaO_2$. Below $x = 0.97$, the structure underwent a 0.4% decrease in cell volume. For compositions rich in Cu, the *a* parameter remained constant while the *c* parameter shrank at a constant rate. Despite these changes in cell dimensions, the results of current-voltage and impedance spectroscopy measurements indicate that both the conductivity and the activation energy do not vary with *x*. The absence of a change in electrical properties as well as the formation of secondary phases in non-stoichiometric compositions suggests that $CuGaO_2$ does not allow significant deviations from the ideal $CuGaO_2$ stoichiometry. This implies that the *p*-type conductivity is fixed by a defect species that does not vary with the Cu stoichiometry.

1. Introduction

Transparent conducting oxides (TCO's) have a wide-variety of applications ranging from transparent electrodes in flat panel displays to coatings on low emissivity architectural glass. As such, a considerable amount of research has been performed in this broad field [1–7] With the advent of *p*-type TCOs [8], the possibility of a transparent *pn*-junction, and thus transparent ceramic electrical devices has become a reality [1, 9, 10]. The current industry standard for *n*-type TCOs is tin-doped indium oxide (ITO). Typically, ITO has a conductivity of at least 1000 S/cm while transparent delafossites have achieved *p*-type conductivities of only 220 S/cm with Mg-doped $CuCrO_2$ [11]. Clearly, the conductivity values for *p*-type delafossites must be improved if they are to have any commercial viability. In order to further improve the electrical characteristics of $CuGaO_2$, a better understanding of the conduction mechanisms is required. This work attempts to further this task by examining the defect chemistry of $CuGaO_2$ as it relates to the structural and electrical properties by creating and characterizing non-stoichiometric compounds based on Cu_xGaO_2.

The delafossite structure has the chemical formula of ABO_2, where the nominal oxidation states for each ion are A^{1+}, B^{3+}, and O^{2-}. It can form either hexagonal 2H ($P6_3/mmc$) or rhombohedral 3R ($R\bar{3}m$) structures, however the majority of delafossites (including $CuGaO_2$) exhibit the 3R structure (Fig. 1). The delafossite structure has the coordination scheme $A^{II}B^{VI}O_2^{IV}$, where the A-site is a monovalent cation (Cu, Ag, Pd, and Pt), while the B-site is a trivalent cation (Al, Co, Cr, Ga, In, etc.) [12–14]. Fig. 1 shows the delafossite crystal structure which can be described as sheets of edge shared BO_6 octahedra separated by triangular layers of A-ions. The B^{3+} atom is a six-fold coordinated ion and the A^+ ions form linear O-A-O units oriented parallel to the *c* axis [15]. It should be noted that the BO_6 units are not perfect octahedra; rather they are slightly flattened along the *c* axis. This distortion is likely due to the electrostatic repulsion of the neighboring B^{3+} ions [16]. A summary of Cu-based delafossites and their respective conductivities can be seen in Table I.

There has been limited success in using cation doping and oxygen intercalation to improve the conductivity of delafossites [1, 10, 11, 17–21]. Typically, doping to increase the conductivity does so at the expense of transparency. For example, $CuGaO_2$ thin films have been doped with Fe to increase conductivity from 0.02 S/cm to 1 S/cm, however optical transparency decreased from 70–85% to 50–70% [11].

The defect structure plays a considerable role in determining the conductivity of delafossites. For most *p*-type delafossite compounds, the *p*-type conductivity arises in the absence of intentional doping. Drawing upon the known defect chemistry of Cu_2O [22] it has been theorized that a combination of ionized copper vacancies (V'_{Cu}) andinterstitial oxygens (O''_i) are the

*Author to whom all correspondence should be addressed.

TABLE I Conductivities and activation energy of a selection of Cu-delafossites

Material	Reference	σ (S/cm)	E_A (eV)	Type
$CuAl_xO_y$	28	200	–	Film
$CuAlO_2$	24	0.3	0.2	Film
$CuAlO_2$	29	17	0.19	Bulk
$CuCrO_2$	30	100	0.36	Bulk
$CuCrO_2$:Mg	11	220	0.02	Film
$CuEuO_{2.65}$	31	0.065	0.24	Bulk
$CuFeO_2$	32	1.5	0.17	Bulk
$CuFeO_2$:Mg	32	9.0	0.11	Bulk
$CuFeO_2$:Sn	32	0.32	0.10	Bulk
$CuGaO_2$	11	0.02	0.1	Film
$Cu(Ga_{0.5}Fe_{0.5})O_2$	11	1	0.1	Film
$CuGaO_2$:Ca	33	55	0.24	Bulk
$CuInO_2$:Ca	10	0.0028	0.19	Film
$CuInO_2$:Sn	10	0.0038	0.077	Film
$CuLaO_{2.64}$	31	0.012	0.24	Bulk
$CuNi_{2/3}Sb_{1/3}O_2$	11	0.05	0.7	Film
$CuNdO_{2.62}$	31	2.0	0.24	Bulk
$CuPrO_{2.62}$	31	0.13	0.24	Bulk
$CuScO_{2+x}$:Mg	11	30	0.095	Film
$SrCu_2O_2$:K	1	0.048	0.1	Film
$CuSmO_{2.63}$	31	0.22	0.24	Bulk
$CuYO_{2.47}$:Ca	31	0.0078	0.24	Bulk
$CuYO_2$	34	0.000001	–	Bulk
$CuYO_{2.58}$	31	0.00085	0.24	Bulk
$CuYO_2$:Ca	34	0.0022	0.21	Bulk

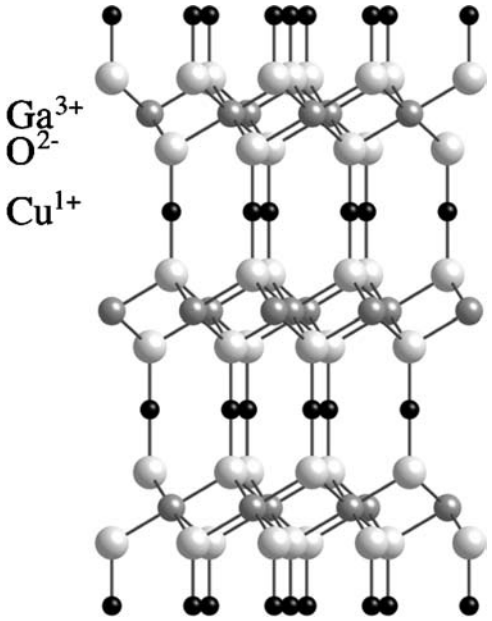

Figure 1 Delafossite crystal structure.

primary defects responsible for *p*-type conductivity in delafossites such as $CuAlO_2$ and $CuGaO_2$ [8, 23, 24]. Evidence for this has been found in the demonstration that oxygen intercalation of $CuScO_2$ and $CuAlO_2$ was shown to improve conductivity at the expense of transparency [11, 25].

Aliovalent doping of $CuGaO_2$ has been largely unsuccessful at either increasing the conductivity or inducing *n*-type conductivity. Acceptor doping with Ni^{2+} or Mg^{2+} did not result in a significant increase in conductivity, and donor doping with Sn^{4+} resulted in a dramatic decrease in conductivity along with the formation of compensating ionic defects in the form of Cu-vacancies [26]. Therefore, the focus of this work is to examine the limits of non-stoichiometry in $CuGaO_2$ and relate the role of Cu-vacancies to the electrical conductivity through Cu_xGaO_2 with a varying concentration of Cu.

2. Experimental

Sintered disks of $CuGaO_2$ were prepared using solid state synthesis. The desired compositions were batched from Cu_2O (99.9%, Alfa-Aesar) and Ga_2O_3(99.999%, All-Chemie). The batched compositions were milled in ethanol for 4 h using zirconia media in a vibratory mill to ensure a homogeneous mixture. The powders were dried and calcined at 1100°C for 12 h in a sealed tube furnace with a flowing N_2/O_2 gas mixture of 0.1% O_2. The calcined powders were quenched from 1100°C by using a magnetic pull-rod to rapidly cool the powders to room temperature while maintaining atmospheric integrity. The powders were then sieved through a 60 μm mesh, and a small amount of polyvinyl acetate (PVA) binder was added. Pellets with a diameter of 12.5 mm were uniaxially pressed. The resulting pellets were fired at 1100°C for 24 h under the conditions (0.1 %O_2), with the addition of a binder burnout step consisting of 6 h at 600°C. The pellets were once again quenched by rapidly removing them from the hot zone of the furnace.

Once the pellets had been fired, each pellet was then ground to a uniform thickness of 1.0 mm and X-ray diffraction (XRD) was employed to analyze the crystal structure. Density measurements were performed on the sintered pellets via Archimedes method. A silver-based electrode paste (Ferro C1000) was painted onto both sides of the pellet and fired at 400°C for 10 min under the same atmosphere as the sintering conditions. Room temperature ac impedance spectroscopy measurements were made using an HP 4194A impedance/gain-phase analyzer, dc current-voltage curves were measured using a Keithley 237 source-measure unit, and resistance versus temperature plots were made using a Delta 9023 environmental chamber. All of the electrical measurements were computer controlled using Labview software. A Siemens D500 diffractometer with a Cu-Kα radiation source was used, and the patterns were analyzed using Jade 6.5 and Unitcell software.

3. Results

3.1. Structural characterization

XRD analysis was performed on Cu_xGaO_2 compositions with x ranging from 0.95 to 1.05 (Figs 2 and 3). Previous authors have shown that a considerable amount of non-stoichiometry can exist on the anion site in some delafossites, e.g. $CuScO_{2+\delta}$ [11]. The oxygen content of the specimens in this work was not determined, however for the purposes of this article the batch compositions will be identified simply by the formula unit Cu_xGaO_2.

For both Cu-deficient and Cu-excess compositions, the 3R delafossite phase was the dominant phase. The secondary phases Cu_2O and Ga_2O_3 were also identified

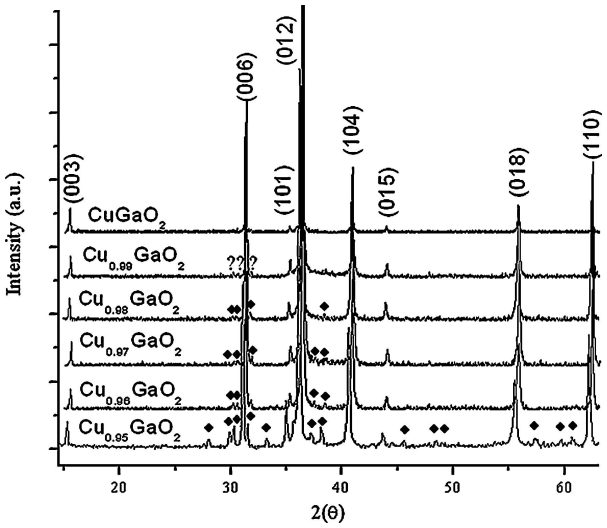

Figure 2 XRD data for Cu-deficient Cu_xGaO_2; ♦ symbol denotes Ga_2O_3 peaks.

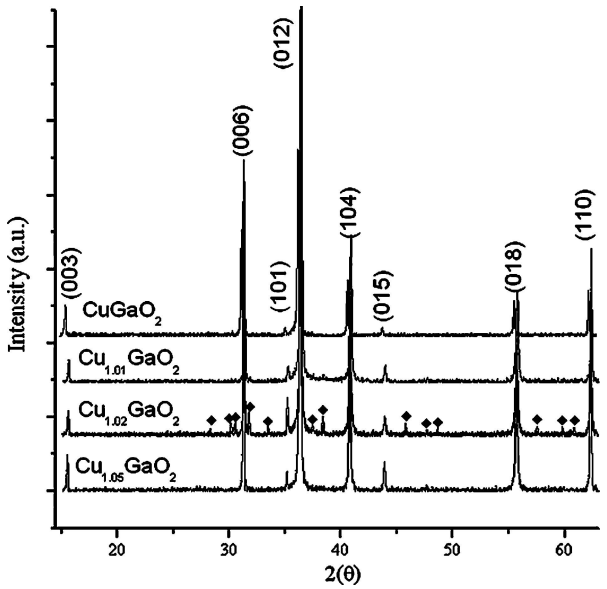

Figure 3 XRD data for Cu-excess Cu_xGaO_2; ♦ symbol denotes Ga_2O_3 peaks.

in some compositions. There were no peaks corresponding to the $CuGa_2O_4$ spinel phase or Cu metal. This suggests that the temperature, oxygen partial pressure, and quench conditions were appropriately targeted for the $CuGaO_2$ phase field.

For the stoichiometric composition, single phase delafossite was observed. For the Cu-deficient compositions, delafossite was still shown to be the dominant phase but small amounts of Ga_2O_3 were observed. The mole fraction of the Ga_2O_3 phase increased with decreasing x. The diffraction patterns from compositions with excess Cu displayed only delafossite peaks up to $x = 1.05$, with the exception of the $x = 1.02$ composition which showed trace amounts of Ga_2O_3. The presence of Cu_2O could not be confirmed in any of the Cu-excess compositions because the primary peak for Cu_2O is overshadowed by the (012) delafossite peak. It should also be noted that there were no trends identified in the width of the (012) delafossite peak as a function of x.

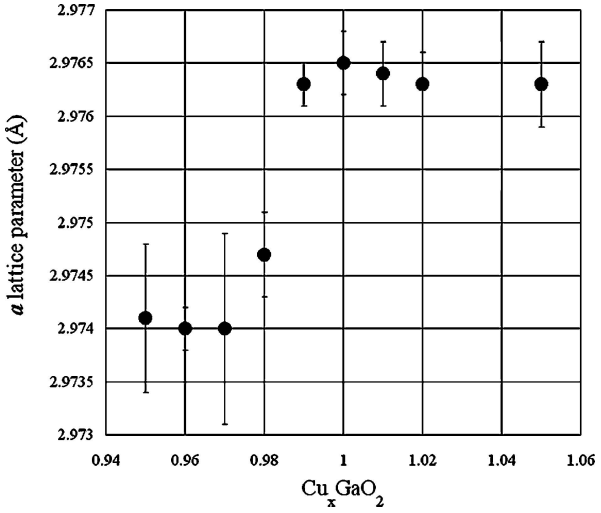

Figure 4 ***a*** lattice parameter versus composition x.

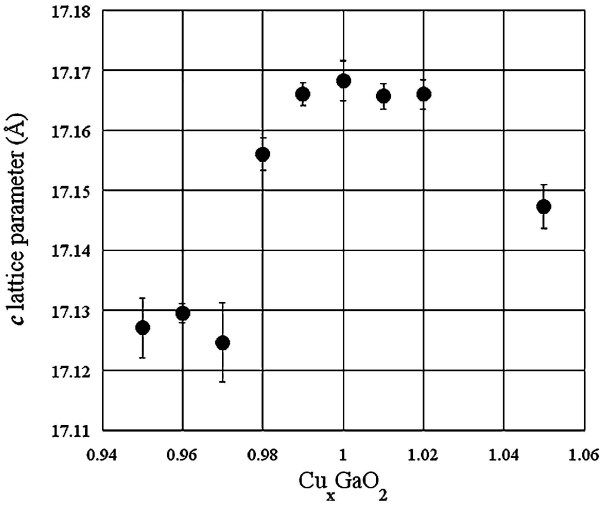

Figure 5 ***c*** lattice parameter versus composition x.

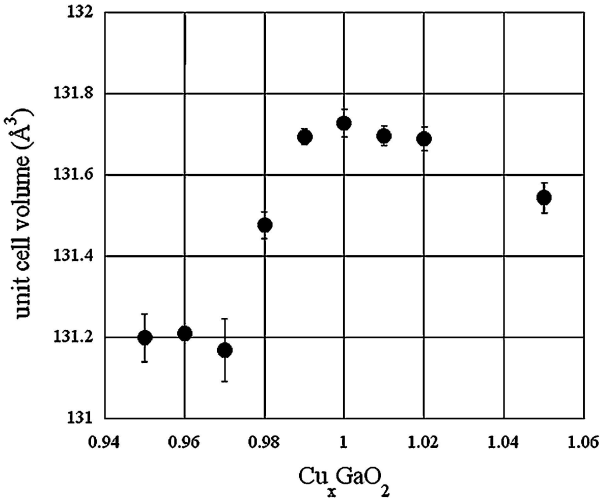

Figure 6 Unit cell volume versus composition x.

The delafossite unit cell dimensions were calculated with a least mean squares determination with the results presented in (Figs 4–6). While the $CuGaO_2$ phase is rhombohedral, the lattice parameter data are presented using the equivalent hexagonal unit cell. These figures show a marked stability in the unit cell dimensions over

TABLE II Phases determined through EDS analysis

Compound	Phases
$Cu_{0.96}GaO_2$	Single Phase + Ga_xO_y
$Cu_{0.97}GaO_2$	Single Phase + Ga_xO_y
$Cu_{0.98}GaO_2$	Single Phase
$Cu_{0.99}GaO_2$	Single Phase
$CuGaO_2$	Single Phase
$Cu_{1.01}GaO_2$	Single Phase
$Cu_{1.02}GaO_2$	Single Phase + Cu_xO_x and Ga_xO_y
$Cu_{1.05}GaO_2$	Single Phase + Cu_xO_x and Ga_xO_y

the compositional range $0.99 \leq x \leq 1.02$. Within the Cu-deficient compositions, the a and c parameter and cell volume all exhibited a marked decrease at $x \leq 0.98$. This coincides with the formation of Ga_2O_3 in the XRD data. Since the a-parameter corresponds most closely to the geometry of the BO_6 octahedral layer, the observed decrease in a may be due to a rearrangement in the B-site occupancy. Additionally, since the c-axis parameter is strongly associated with the O-A-O bonding in the A-site layer, it is likely that the observed decrease in c is related to an increase in vacancies on the A-site.

For Cu-excess compositions, the a-lattice parameter remained relatively constant up to and including the $x = 1.05$ composition. The c parameter decreased to a minimum at $x = 1.05$. These data suggest that the composition of the B-site remained constant up to $x = 1.05$. However, it is not certain why the c parameter decreases with increasing x.

For most compositions, the diffraction peaks for Cu_2O were difficult to identify because of a strong overlap with the delafossite peaks. Therefore, scanning electron microscopy (SEM) with energy dispersive spectroscopy (EDS) was employed to verify the existence of the secondary phases. The results from the EDS study are presented in Table II. No secondary phases could be identified for compositions between $x = 0.98$ and $x = 1.02$. Beyond those limits, Ga-rich and/or Cu-rich oxide phases were observed. Quantitative EDS measurements were not carried out, but it is most likely that the secondary phases observed in the SEM correspond to the Cu_2O and Ga_2O_3 phases identified in the XRD data.

A micrograph showing the typical microstructure of the sintered $CuGaO_2$ pellets is shown in Fig. 7. The sample was etched using a 1M H_2SO_4 solution for 1.5 min. As illustrated in the figure the densities of each pellet ranged from 60–70% of theoretical density. A rough analysis indicated that the grain size was approximately 1 μm, with larger conglomerations forming to the size of 5–10 μm. This structure is indicative of incomplete sintering.

3.2. Electrical measurements

A number of electrode materials were investigated in this study. Fired Ag-electrodes proved to be the best, with a negligible bias-dependence to the electrical properties and a low contact resistance. The electrical measurements taken with Ag-electrodes showed consistent

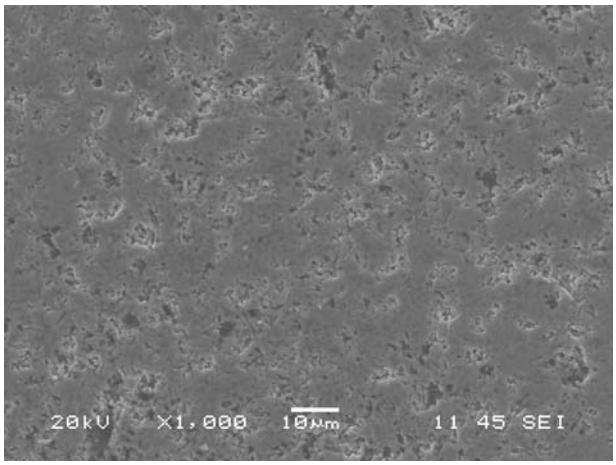

Figure 7 SEM micrograph of typical $CuGaO_2$ microstructure.

resistance values from both ac impedance spectroscopy and dc current-voltage measurements.

The results of dc current-voltage measurements are shown in Table III. While there is some variation in conductivity, the conductivities for all compositions are close to 0.01 S/cm. These values are in close agreement with the other reported conductivities of $CuGaO_2$ which range from 0.005 to 0.063 S/cm [11, 23, 27].

Impedance spectroscopy measurements were used to examine the discrete contributions to the impedance of each compound. Nyquist plots we created by analyzing the real (Z') and imaginary (Z'') impedance of each sample from 100 Hz to 5 MHz. The data can be fit to a relatively simple equivalent circuit (Fig. 8), and used to extrapolate a full model (Fig. 9). This equivalent circuit is commonly used to describe impedance elements arising from grain, grain boundary, and interfacial components. Because of the time constants associated with each element, typically the grain resistance is given by R1, the grain boundary resistance is given as R2, and the interfacial resistance is given by R3. Table IV gives a summary of the results for the compositions in this study. In each of these cases, R1 provided the largest contribution to the overall resistance of the sample. This was closely followed by R2, which provided a lesser but still considerable contribution to the resistance. The R3

TABLE III DC conductivities for Cu_xGaO_2 compounds

Compound	DC σ (S/cm)
$Cu_{0.96}GaO_2$	0.014
$Cu_{0.97}GaO_2$	0.0069
$Cu_{0.98}GaO_2$	0.0071
$Cu_{0.99}GaO_2$	0.016
$CuGaO_2$	0.011
$Cu_{1.01}GaO_2$	0.014
$Cu_{1.02}GaO_2$	0.0057
$Cu_{1.05}GaO_2$	0.016

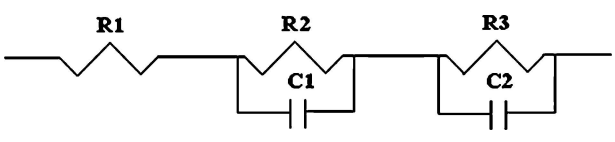

Figure 8 Equivalent circuit used in impedance analysis.

TABLE IV Fitting parameters derived from impedance spectra for Cu_xGaO_2 ceramics using the equivalent circuit shown in Fig. 8

Compound	R1 (Ω)	R2 (Ω)	R3 (Ω)
$Cu_{0.96}GaO_2$	4.63	1.39	0.42
$Cu_{0.97}GaO_2$	4.85	1.64	0.12
$Cu_{0.98}GaO_2$	7.99	3.27	0.22
$Cu_{0.99}GaO_2$	3.54	1.06	0.14
$CuGaO_2$	6.00	2.38	0.27
$Cu_{1.01}GaO_2$	3.27	2.45	0.58
$Cu_{1.02}GaO_2$	9.45	2.63	0.37
$Cu_{1.05}GaO_2$	4.81	1.33	0.24

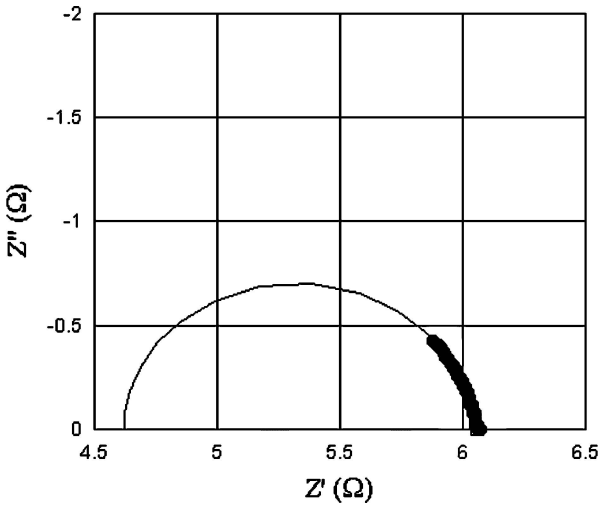

Figure 9 Nyquist plot and equivalent circuit extrapolation.

TABLE V Activation energies for Cu_xGaO_2 compounds in this study

Compound	E_a(eV)
$Cu_{0.96}GaO_2$	0.20
$Cu_{0.97}GaO_2$	0.22
$Cu_{0.98}GaO_2$	0.21
$Cu_{0.99}GaO_2$	0.20
$CuGaO_2$	0.21
$Cu_{1.01}GaO_2$	0.18
$Cu_{1.02}GaO_2$	0.21
$Cu_{1.05}GaO_2$	0.21

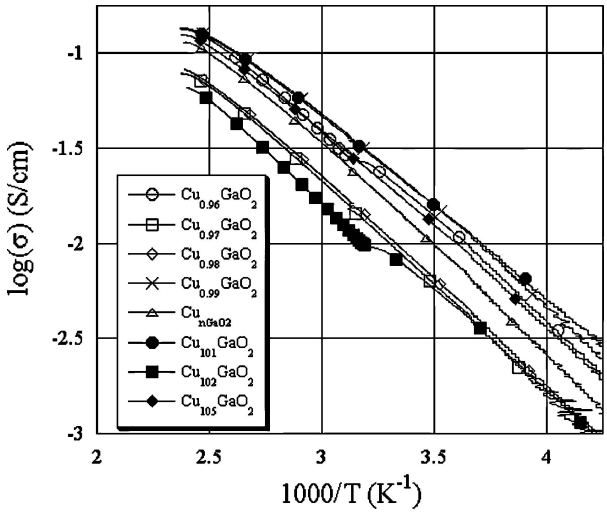

Figure 10 Temperature dependence of conductivity for Cu_xGaO_2 compounds.

resistance of each sample contributed a relatively minor fraction of less than 10% of the total resistance. It is important to note that grain size effects can be neglected because SEM observations indicated that the grain size remained relatively constant across all compositions. The most important conclusion that can be drawn from the data is that all of the compositions in this study exhibited a similar impedance spectra. In combination with the dc electrical data, this suggests that the electrical conductivity was remarkably invariant to composition.

The temperature dependence on conductivity was also explored. By examining the change in conductivity from 150 to −50°C, one can see an approximately linear relationship when plotting log σ versus reciprocal temperature for each of the compounds (Fig. 10). The activation energy (E_A) of each compound can also be obtained using the Arrhenius equation:

$$\ln \sigma = \ln \sigma_0 + \frac{-E_A}{k_B T} \tag{1}$$

The activation energies of each compound can be found in Table V. The activation energies ranged from 0.18–0.22 eV with no discernable trend.

4. Discussion

The combination of XRD and SEM/EDS data suggests that the solid state synthesized $CuGaO_2$ delafossite ceramics tolerates very little variation in the Cu non-stoichiometry in Cu_xGaO_2. The data illustrate that there exists a compositional range between approximately $Cu_{0.99}GaO_2$ to $Cu_{1.02}GaO_2$ where the unit cell dimensions remain constant. The implication is that the composition of the delafossite phase over the range $0.99 \leq x \leq 1.02$ does not change, and the mole fractions of Cu- or Ga-oxides required for mass balance appear in the form of a secondary phase. A marked change in the unit cell dimensions occurs below $x = 0.97$, where the cell volume decreases by approximately 0.4%. The Cu-excess compositions exhibited a smooth decrease in volume down to the $x = 1.05$ composition.

The electrical transport properties of the compounds did not exhibit a dependence on x. While most of the compositions in this study are not single phase, it is expected that the electrical properties would be dominated by the large mole fraction of the delafossite phase. Both secondary phases, Ga_2O_3 and Cu_2O, appear in small amounts and are both relatively insulating compared to $CuGaO_2$. The compositional invariance seen in the electrical data also supports the conclusion that the delafossite phase has no tolerance for Cu non-stoichiometry. The close correspondence between the activation energies across a wide range in x provides further support for this conclusion. It is interesting to note that even at $x = 0.97$ where the cell parameters exhibit a significant shift, the electrical properties of the material remain constant.

These results are relevant to conduction mechanisms which are responsible for the observed p-type behavior in most Cu delafossites. Previous workers have

suggested V'_{Cu}, O''_i, and $(Al_{Cu}{}^{\bullet\bullet}2O''_i)''$ as the primary defect species for *p*-type $CuAlO_2$ which is the most well-characterized delafossite material. In this study, it is clearly apparent that it is not possible to introduce significant variations in the stoichiometry of the structure through high temperature solid state synthesis techniques. It is possible that Cu-vacancies can be stabilized in thin film samples prepared through non-equilibrium processes. It is not clear whether or not interstitial oxygens can be responsible for the observed results. The oxygen content of the samples in this study was not measured, however all of the samples were prepared under identical conditions (pO_2, T). It has been proposed by Ingram *et al.* [25] that the most energetically favorable site for the interstitial oxygen is within the 2-dimensional A-layer in the basal plane.

In $CuAlO_2$, it has been demonstrated that the Cu/Al stoichiometry has a significant effect on the conductivity. The model of Ingram *et al.* for $CuAlO_2$ proposes that an intrinsic acceptor defect associate ($(Al_{Cu}{}^{\bullet\bullet}2O_i{}'')''$) with tetrahedrally coordinated Al on the Cu-site determines the hole concentration. The concentration of this defect associate appears to be dependent on the Cu/Al stoichiometry in $CuAlO_2$. Considering the feasibility of this defect existing in $CuGaO_2$, the *a* lattice parameter that scales with the interatomic spacing in the basal plane is 4.2% larger than $CuAlO_2$. However, the ionic radius of Ga^{3+} in a tetrahedral coordination is 15.1% larger than Al^{3+}. Therefore, this defect species may be less energetically favorable in $CuGaO_2$ than in $CuAlO_2$. In the solid state synthesized specimens in this work, it was not possible to modify the Cu/Ga non-stoichiometry. If the hole concentration depended on the concentration of this defect complex, since the conductivity of Cu_xGaO_2 was observed to be independent of x it is likely that the defect concentration was also independent of x.

5. Conclusions

Non-stoichiometric compounds of Cu_xGaO_2 ranging from $Cu_{0.95}GaO_2$ to $Cu_{1.05}GaO_2$ were prepared using high temperature solid-state synthesis. From XRD, SEM/EDS, and electrical measurements it was observed that the $CuGaO_2$ structure does not allow significant deviations in the Cu-stoichiometry. XRD refinement shows the lattice parameters remains invariant from $Cu_{0.99}GaO_2$ to $Cu_{1.02}GaO_2$. Below $x = 0.97$ there is a contraction in both the *a* and *c* parameters. The Cu-excess compositions exhibited a decrease in the *c* parameter with x, while the *a* parameter remained constant.

dc conductivity, ac impedance, and conductivity versus temperature measurements showed that the conductivity remained constant across the entire compositional range. The magnitude of the conductivity was approximately 0.01 S/cm and the activation energies ranged from 0.18–0.22 eV. Impedance spectra from each composition could be fit to a single equivalent circuit and the magnitude of the resistance and capacitance of the circuit elements did not varywith x. All of the above results suggest that primary defect species responsible for the *p*-type conductivity in $CuGaO_2$ could not be manipulated by varying the Cu/Ga ratio in solid state synthesized ceramics.

Acknowledgements

This work was supported by the National Science Foundation under grant DMR-0093616.

References

1. H. KAWAZOE, H. YANAGI, K. UEDA and H. HOSONO, *MRS Bull.* **25** (2000) 28.
2. B. G. LEWIS and D. C. PAINE, *ibid.* **25** (2000) 22.
3. D. S. GINLEY and C. BRIGHT, *ibid.* **25** (2000) 15.
4. R. G. GORDON, *ibid.* **25** (2000) 52.
5. T. MINAMI, *ibid.* **25** (2000) 38.
6. J. FREEMAN, K. R. POEPPELMEIER, T. O. MASON, R. P. H. CHANG and T. J. MARKS, *ibid.* **25** (2000) 45.
7. T. J. COUTTS, D. L. YOUNG and J. LI, *ibid.* **25** (2000) 58.
8. H. KAWAZOE, *et al.*, *Nature (London)* **389** (1997) 939.
9. A. KUDO, *et al.*, *Appl. Phys. Lett.* **75** (1999) 2851.
10. H. YANAGI, *et al.*, *Solid State Commun.* **121** (2001) 15.
11. J. TATE, *et al.*, *Thin Solid Films* **411** (2002) 119.
12. R. D. SHANNON, D. B. ROGERS and C. T. PREWITT, *Inorg. Chem.* **10** (1971) 713.
13. R. D. SHANNON, D. B. ROGERS, C. T. PREWITT and J. L. GILLSON, *ibid.* **10** (1971) 723.
14. R. D. SHANNON, C. T. PREWITT and D. B. ROGERS, *ibid.* **10** (1971) 719.
15. H. C. KANDPAL and R. SESHADRI, *Solid State Sci.* **4** (2002) 1045.
16. A. BULJAN, P. ALEMANY and E. RUIZ, *J Phys. Chem. B* **103** (1999) 8060.
17. D. R. KAMMLER, *et al.*, *Proc.—Electrochem. Soc.* **99** (11) (1999) 68.
18. R. NAGARAJAN, *et al.*, *Intern. J. Inorg. Mater.* **3** (2001) 265.
19. X. NIE, S.-H. WEI and S. B. ZHANG, *Phys. Rev. Lett.* **88** (2002) 066405/1.
20. R. NAGARAJAN, S. UMA, M. K. JAYARAJ, J. TATE and A. W. SLEIGHT, *Solid State Sci.* **4** (2002) 787.
21. M. TRARI, *et al.*, *Annales de Chimie (Paris)* **19** (1995) 521.
22. O. PORAT and I. RIESS, *Solid State Ion.* **81** (1995) 29.
23. K. UEDA, T. HASE, H. YANAGI, H. KAWAZOE and H. HOSONO, *J App. Phys.* **89** (2001) 1790.
24. H. YANAGI, *et al.*, *ibid.* **88** (2000) 4159.
25. B. J. INGRAM, G. B. GONZALEZ, T. O. MASON, D. SHAHRIARI, A. BERNABÈ, D. KO and K. POPPELMEIER, *Chem. Mater.* **16** (2004) 5616.
26. R. B. GALL and D. P. CANN, *Ceram. Enging Sci. Proc.* **24** (2003) 143.
27. H. YANAGI, H. KAWAZOE, A. KUDO, M. YASUKAWA and H. HOSONO, *J. Electro.* **4** (2000) 407.
28. L. F. JOHNSON, M. B. MORAN, E. SAVRUN, M. SARIKAYA and R. R. KOLEGA, *Mater. Res. Soc. Symp. Proc.* **623** (2000) 271.
29. F. A. BENKO and F. P. KOFFYBERG, *J. Phys. Chem. Solids* **45** (1984) 57.
30. Idem., *Mater. Res. Bull.* **21** (1986) 753.
31. K. ISAWA, *et al.*, *Phys. Rev. B: Cond. Matter* **56** (1997) 3457.
32. F. A. BENKO and F. P. KOFFYBERG, *J. Phys. Chem. Solids* **48** (1987) 431.
33. F. A. BENKO and F. P. KOFFYBERG, *Physica Status Solidi A: Appl. Res.* **94** (1986) 231.
34. F. A. BENKO and F. P. KOFFYBERG, *Canadian J. Phys.* **63** (1985) 1306.

Received 1 September 2004
and accepted 2 March 2005